Noise-Enabled Precision Measurements of a Duffing Nanomechanical Resonator

J. S. Aldridge and A. N. Cleland

Department of Physics, University of California at Santa Barbara, Santa Barbara, California 93106, USA

(Received 21 May 2004; published 19 April 2005)

We report quantitative measurements of the nonlinear response of a radio frequency mechanical resonator with a very high quality factor. We measure the noise-free transitions between the two basins of attraction that appear in the nonlinear regime, and find good agreement with theory. We measure the transition rate response to controlled levels of white noise, and extract the basin activation energy. This allows us to obtain precise values for the relevant frequencies and the cubic nonlinearity in the Duffing oscillator, with applications to parametric sensing.

DOI: 10.1103/PhysRevLett.94.156403 PACS numbers: 85.85.+j, 62.25.+g, 62.30.+d

Doubly clamped mechanical resonators have recently been the subject of much attention due to their ability to make very high frequency, high quality factor resonators, with applications in weak force and small mass detection, frequency stabilization, and possibly quantum computation [1–14]. The limit for parametric sensing is often set by the precision with which a resonator parameter, such as the mass, can be monitored, limited typically by measurement and intrinsic noise sources. Here we show how one can use the intrinsic nonlinear response of these resonators, and the addition of external broadband noise, to significantly improve the measurement precision of two such parameters, the resonance frequency and the cubic nonlinearity. This has direct implications for the ultimate sensitivity of such parametric sensors.

At large drive amplitudes, doubly clamped resonators exhibit a bistable response quantitatively similar to the Duffing oscillator [15,16]. The motion in the fundamental mode of a doubly clamped beam is well approximated by the Duffing equation, which for a natural resonance frequency Ω_0 and quality factor Q, driven at frequency Ω, has the form

$$M\frac{d^2Y}{dt^2} + M\frac{\Omega_0}{Q}\frac{dY}{dt} + M\Omega_0^2 Y + KY^3 = \mathcal{B}\cos(\Omega t) + \mathcal{B}_n(t), \tag{1}$$

where Y denotes the displacement amplitude of the midpoint of the beam, M the mass of the beam, $\mathcal{B}$ the amplitude of the external driving force, and $\mathcal{B}_n(t)$ the stochastic forcing function due to thermal and external noise [6,15,16]. This assumes that the beam oscillates in the mode with natural frequency Ω_0, that the displacement $Y(t)$ is the only relevant degree of freedom, and that the equation of motion includes only the third-order nonlinearity, with strength K. There are a number of systems that are modeled by the Duffing equation, including analog circuits [17], a relativistic electron in a magnetic field [18], and the current-biased Josephson junction [19]. The present experiment is one of the first quantitative tests of the theory that describes transitions between stable states of the Duffing oscillator.

The displacement $Y(t)$ in Eq. (1) can be written [20] as

$$Y(t) = U_1(t)\cos(\Omega t) + U_2(t)\sin(\Omega t), \tag{2}$$

in terms of the two quadrature amplitudes $U_{1,2}(t)$. For a high Q system driven at frequency Ω near Ω_0, the slowly varying envelope approximation can be used [15,20], where the functions $U_{1,2}(t)$ are replaced by their slowly varying averages, $u_{1,2}(t)$, respectively.

The average functions $u_{1,2}(t)$ satisfy the equations of motion

$$\begin{aligned}\frac{du_1}{dt} &= \frac{1}{2}\left[-\frac{1}{\Omega}(\Omega^2-\Omega_0^2)u_2 + \frac{3}{4}\frac{K}{M\Omega}u_2(u_1^2+u_2^2) - \frac{\Omega_0}{Q}u_1 + \frac{\mathcal{B}_{n1}(t)}{M\Omega}\right],\\ \frac{du_2}{dt} &= \frac{1}{2}\left[\frac{1}{\Omega}(\Omega^2-\Omega_0^2)u_1 - \frac{3}{4}\frac{K}{M\Omega}u_1(u_1^2+u_2^2) - \frac{\Omega_0}{Q}u_2 + \frac{\mathcal{B}}{M\Omega} + \frac{\mathcal{B}_{n2}(t)}{M\Omega}\right],\end{aligned} \tag{3}$$

with independent noise functions $\mathcal{B}_{n1}(t)$ and $\mathcal{B}_{n2}(t)$.

The Duffing oscillator exhibits one stable state for small drive amplitudes $\mathcal{B}$, while above a critical amplitude $\mathcal{B}_c$ a bifurcation occurs, creating two stable basins of attraction. One basin corresponds to larger displacement amplitudes, and is stable for drive frequencies up to an upper critical frequency ν_U ($\nu = \Omega/2\pi$), determined by the drive amplitude $\mathcal{B}$. The other stable basin has a smaller displacement amplitude, and is stable for frequencies down to a lower critical frequency ν_L, also determined by the drive amplitude. There are three equilibrium points in Eq. (3); two of these are stable foci, and the third is a metastable saddle point.

A transition between the two basins occurs in the absence of noise when the activation energy separating them is reduced to zero by changing either the drive amplitude or the drive frequency. In the presence of noise, however, the Duffing oscillator exhibits stochastic transitions between the two basins. For weak noise, the transitions are very rare except near the critical frequencies $\nu_{L,U}$, while, as the noise

power is increased, the separation between the upper and lower transition frequencies is effectively reduced.

Here we make detailed measurements of the nonlinear dynamics of a doubly clamped beam, investigating both the dynamical motion and the change in the interbasin transition rates due to broadband noise. Our experimental system comprises a pair of doubly clamped beams of single-crystal aluminum nitride, with dimensions $3 \times 0.2 \times 0.14\ \mu\text{m}^3$, oriented perpendicular to one another and fabricated together on a chip of single-crystal Si. The fabrication technique is described elsewhere [21]. The chip was placed in the vacuum bore of an $B = 8$ T magnet at 4.2 K, with one beam (the active beam) oriented perpendicular to the field direction, the other (reference) beam parallel to the field. Magnetomotive actuation and displacement detection was used to drive the active beam [1], where the parallel orientation of the reference beam decouples it from the drive force (see Fig. 1). The active beam had a natural resonance frequency $\nu_0 = \Omega_0/2\pi = 92.9$ MHz, a quality factor $Q = 6750$, and a critical drive power for inducing the hysteretic bifurcation of -61 dBm. Using the beam resistance of 11 Ω, this corresponds to a critical drive force $\mathcal{B}_c = 580$ pN and a midpoint displacement of 18 nm.

Measurements were made with a radio frequency (rf) bridge [22], as shown in Fig. 1(a). The rf drive signal is split by a 180° phase splitter, with the two phases passing through separate stainless coaxial cables of similar construction. The 180° phase-shifted signal is connected to one end of the reference beam, and the 0° signal connected to one end of the active beam. The other ends of the two beams are connected to a third coaxial cable that returns to room-temperature electronics. The bridge can be balanced in both amplitude and phase over the range of frequencies used in this experiment, and is typically tuned so that the electrical signal is proportional to the displacement-induced electromotive force [1].

The signal is the demodulated output of the bridge, giving the in-phase and out-of-phase quadrature signals $i(t)$ and $q(t)$. These are proportional, to within a phase factor, to the average amplitudes $u_{1,2}(t)$ [1,22]. In Figs. 1(b)–1(d) we display the responses of the active beam to a range of drive amplitudes, where the frequency is swept through the resonance for each amplitude; the responses are in quantitative agreement with that expected.

In Fig. 2 we compare the measured quadrature amplitudes to numerical solutions of Eq. (3). In Fig. 2(a) we show the calculated phase-space trajectories, and in 2(b) and 2(c) the experimentally measured trajectories. In Figs. 2(d) and 2(e) the time traces are shown for the switching transitions. The correspondence between is apparent, with the trajectories in Fig. 2(a) showing noise-free relaxations to both foci, corresponding to the single-focus transitions measured separately in Figs. 2(b) and 2(c). As the drive frequency is varied, the stable points follow a circle on the $u_{1,2}$ plane, even with the Duffing nonlinearity. These circles are evident in Fig. 1(d).

We now discuss the noise-induced transitions between the foci. Thermally activated escape from a single basin of attraction is a thoroughly studied problem [23,24]. The escape rate over a barrier E_B is given by $\Gamma = a(Q)\nu_0 \times \exp(-E_B/k_BT)$, determined predominantly by the Arrhenius factor and less so by the prefactor $a(Q)$. In our system, there is a basin of attraction about each of the two foci found on a Poincaré map of the configuration space. Instead of a one-dimensional potential well, there is a quasipotential, with dynamics governed by the noise energy at each point in the configuration space [25]. The equivalent activation energy, E_A, for transitions between the foci, is found by integrating the minimum noise energy over the trajectory.

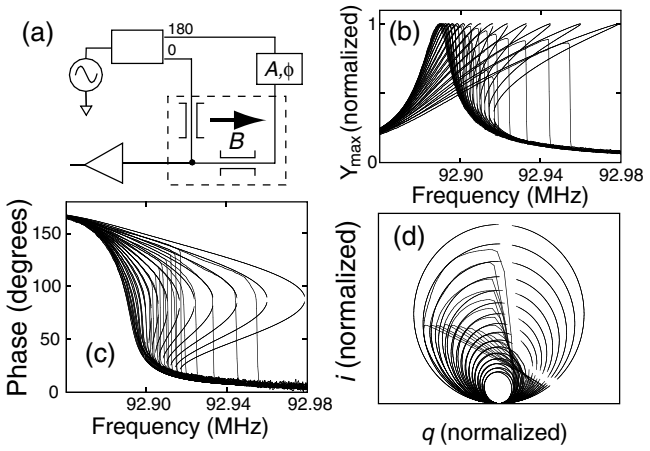

FIG. 1. (a) Circuit and active and reference beams; dotted outline encloses cryogenic part of experiment. Box labeled 0, 180 is a 180° phase splitter, and that labeled A, ϕ allows adjustment of amplitude and phase. Arrow indicates B field orientation. (b) Amplitude versus frequency for drive from -68 to -53 dBm, in 1 dBm steps. (c) Phase for the same drive amplitudes as (b). (d) Hysteresis in $u_1 - u_2$ plane, plotted as i vs q in dimensionless units.

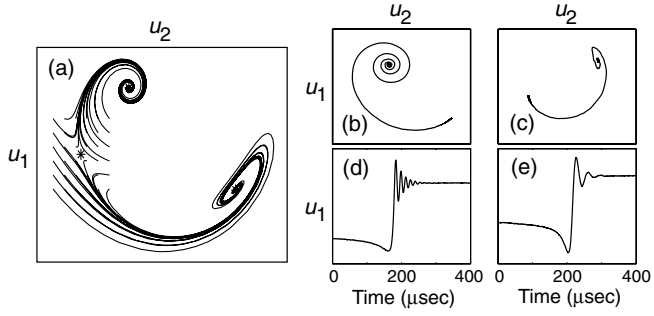

FIG. 2. (a) Numerically generated phase-space flow for a drive force 9 dB above the critical point $\mathcal{B}_c$, and drive frequency 40 kHz above $\Omega_0/2\pi$. Flow begins near the saddle point and evolves toward either focus. (b) Experimental phase-space mean trajectory from focus 1 to focus 2 (8000 averages). (c) Data for phase-space mean trajectory from focus 2 to focus 1 (8000 averages). (d),(e) Experimental time traces for the two switching transitions (8000 averages).

Transitions were induced by using an external white noise signal $\mathcal{B}_n$ combined with the drive signal $\mathcal{B}$. Typical noise powers ranged from -130 to -100 dBm/Hz. The drive was produced by a low noise source, although with no additional noise, the remnant phase noise still induced transitions. The thermal and mechanical noises associated with the finite Q are estimated to be 70 dB below the source noise, too small to induce measurable transitions.

Transition histograms were measured by applying a drive signal to the resonator above the critical value, preparing the resonator in one basin of attraction, and monitoring the switching transition to the other basin. We measured histograms of the switching probability per unit frequency, $h(\nu)$, by sweeping the drive frequency $\nu = \Omega/2\pi$ slowly at a rate $s = d\nu/dt$, and recording the drive frequency at which a transition occurred. The sweep rate was kept low enough that the resonator was always in quasiequilibrium. This technique has been used for measuring switching in current-biased Josephson junctions [26]. The transition rate $\Gamma(\nu)$ is extracted from the histogram $h(\nu)$ using $\Gamma(\nu) = [1 - \int_0^\nu h(\nu')d\nu']^{-1} s h(\nu)$.

In Fig. 3(a) we display a set of histograms $h(\nu)$; higher noise powers shift the peak switching frequency and also broaden the distribution. In Fig. 3(b) we show the transition rates extracted from these histograms, demonstrating the rapid increase in the transition rate as the noise power is increased. We then extract the activation energy $E_A(\nu)$, by inverting the thermal activation expression $\Gamma(\nu) \equiv \Gamma_0 \exp[-E_A(\nu)/k_B T_{\text{eff}}]$, where the effective temperature T_{eff} is proportional to the noise power, and the prefactor Γ_0 is related to the Kramers low-dissipation form [23], $\Gamma_0 \approx \nu_0/Q$. In this technique, the histograms are only logarithmically sensitive to Γ_0, so a precise value is not essential. In Fig. 3(c) we display the activation energy $E_A(\nu)$ extracted from the histograms, showing the expected decline in the activation energy as the drive frequency approaches the critical frequency. The distributions shown in Fig. 3(b) are seen to collapse onto a single curve $E_A(\nu)$. In Fig. 4(a) we show experimentally measured $E_A(\nu)$ curves for transitions from focus 1 to 2 and from 2 to 1, for different drive amplitudes.

We calculated the activation energies numerically [17]. The dynamic solutions to Eq. (1) without noise give the relaxation from the saddle point to one of the foci. During a noise-induced transition, the system is excited from a basin near a focus *towards* the saddle point, which it crosses and then relaxes to the other focus, for which there is an infinite number of trajectories. Given a trajectory, one can calculate the contribution of the noise force using Eq. (1). The energy transferred to the resonator is found by integrating the noise power along the trajectory, yielding the effective activation energy between the foci. The energy transferred is an actionlike quantity, and the most likely escape trajectory is that with the minimum action. The actionlike integral S of the system [27] is then

$$S = \frac{Q}{4\Omega_0 M^2} \int_{\text{path}} \mathcal{B}_n^2(t) dt. \tag{4}$$

The most likely path $Y_0(t)$ minimizes S, and travels near the saddle point. The oscillator evolves from this point to either focus without contributing to the integral, as this relaxation does not require a noise term. Only when the oscillator is evolving against the dissipative flow field, from a focus toward the saddle point, will it contribute to the action integral.

We used a numerical minimization of the trajectories $Y(t)$, using S as a test function to approach the extremum $Y_0(t)$. The trajectories were calculated in the rotating frame, using the relaxation method [28], for different drive

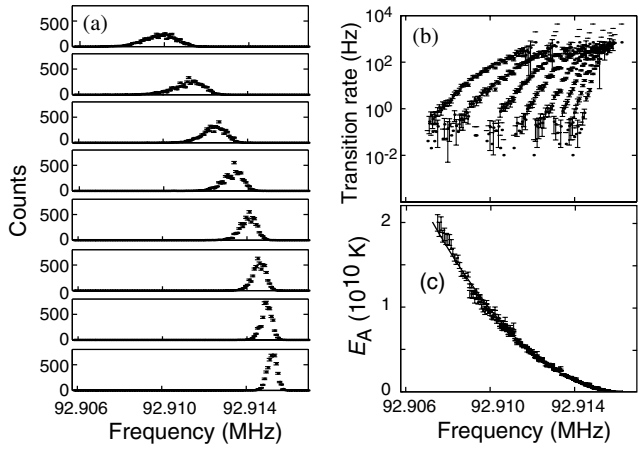

FIG. 3. (a) Switching histograms $h(\nu)$ for different noise powers, with $\mathcal{B} = -56$ dBm, for $1 \rightarrow 2$ transitions. Noise intensity is increased from bottom to top. (b) Transition rates $\Gamma(\nu)$ extracted from switching histograms. (c) Calculated activation energy $E_A(\nu)$ extracted from transition rates and variation in noise power. The noise power was varied from -127 to -113 dBm/Hz. Solid curve is fit to expected dependence.

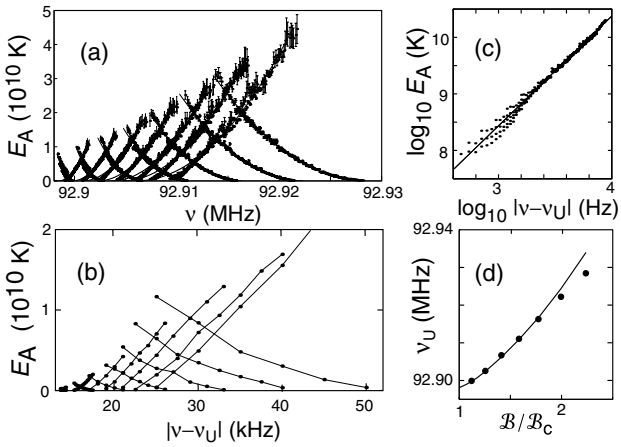

FIG. 4. (a) Measured activation energy for drive force ranging from 1 to 7 dB above $\mathcal{B}_c$. (b) Numerically calculated activation energies between foci 1 and 2. (c) Log-log plot showing $E_A \propto (\nu - \nu_U)^2$ dependence near the critical point. (d) ν_U versus drive amplitude $\mathcal{B}/\mathcal{B}_c$. At large amplitudes the data diverge from the analytic form.

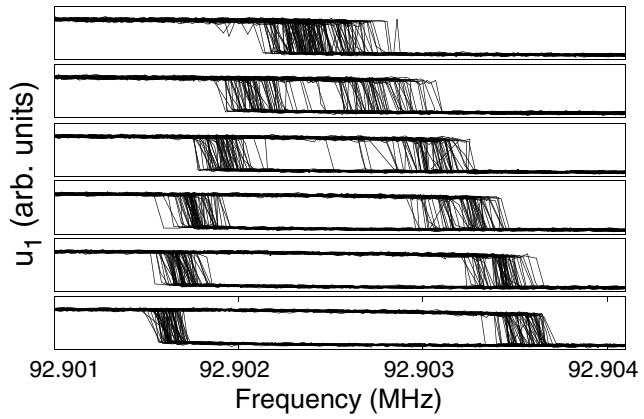

FIG. 5. Amplitude hysteresis plots, for no noise power (bottom), with the drive amplitude set at -59 dBm, 2 dB above the critical point. Noise power was increased by 2 dB for each succeeding frame.

frequencies and amplitudes, yielding the results shown in Fig. 4(b). We find logarithmic agreement between the measured and calculated energies. The largest uncertainty is the noise power coupling efficiency, which is difficult to measure precisely, giving the experimental energy an uncertainty of about a factor of 2.

Near the critical drive power $\mathcal{B}_c$, on the line of the kinetic phase transition, where the activation energies for both transitions are equal, analytic forms indicate the activation energy should have a quadratic dependence [20], $E_A \propto (\nu - \nu_c)^2$, where ν_c is the critical frequency where the energy required for either transition drops to zero. Our measurements demonstrate that, near the critical frequency, the dependence of the activation energy on $|\nu - \nu_U|$ is also quadratic, as shown in Figs. 3(c) and 4(a). This allows a determination of ν_U for a given drive power; our histograms yield an uncertainty of $\Delta\nu_U/\nu_U \approx 3 \times 10^{-7}$. By comparing the observed dependence of ν_U on drive power with that obtained from the numerical analysis, shown in Fig. 4(d), we can extract the natural resonance frequency ν_0 and the coefficient of nonlinearity K. We find $\nu_0 = 92\,887\,360 \pm 10$ Hz and $K = (3745 \pm 4) \times 10^{11}$ N/m^3. Note the numerical analysis has a theoretical uncertainty of $\propto Q^{-2}$. Because Q is constant, this systematic error does not affect the precision of the measurement.

The frequency measurement represents a relative precision of $\Delta\nu_0/\nu_0 \approx 1.1 \times 10^{-7}$. In the linear regime, the resonance frequency can be determined to about one-tenth the resonance width, ν_0/Q; for our resonator, this corresponds to $\Delta\nu_0/\nu_0 \approx 10^{-5}$. This 100-fold improvement in frequency resolution has implications for, e.g., mass sensing with mechanical resonators [2,29].

These measurements were made in the small noise limit, with noise energies much less than the activation energy. At higher noise powers, the hysteresis can be quenched, by rapid noise-induced transitions between the two foci, as shown in Fig. 5: As the noise power is increased, the hysteresis loop grows smaller, until, at the highest powers, the switching is no longer hysteretic. In this limit, the oscillator generates random telegraph signals as it makes transitions. The spectrum of the telegraph signal is related to the transition rate.

In conclusion, we have measured the average escape paths and transition rates between the bistable states of a nonlinear resonator. These measurements are in good agreement with numerical simulations. Detailed analysis allows quantitative measurement of the activation energy between the foci, and provides a sensitive measurement of the resonance frequency and the nonlinear parameter.

We thank C. S. Yung, R. G. Knobel, D. R. Schmidt, L. J. Swenson, and D. K. Wood. This work was funded by the DARPA-DMEA Center for Nanoscience Innovation for Defense.

[1] A. N. Cleland and M. L. Roukes, Appl. Phys. Lett. **69**, 2653 (1996).
[2] K. L. Ekinci *et al.*, Appl. Phys. Lett. **84**, 4469 (2004).
[3] B. Ilic *et al.*, Appl. Phys. Lett. **77**, 450 (2000).
[4] D. S. Greywall *et al.*, Phys. Rev. Lett. **72**, 2992 (1994).
[5] D. W. Carr *et al.*, Appl. Phys. Lett. **75**, 920 (1999).
[6] A. N. Cleland and M. L. Roukes, J. Appl. Phys. **92**, 2758 (2002).
[7] R. G. Knobel and A. N. Cleland, Nature (London) **424**, 291 (2003).
[8] A. D. Armour *et al.*, Phys. Rev. Lett. **88**, 148301 (2002).
[9] K. L. Ekinci *et al.*, J. Appl. Phys. **95**, 2682 (2004).
[10] S. M. Carr *et al.*, Phys. Rev. B **64**, 220101 (2001).
[11] K. L. Turner *et al.*, Nature (London) **396**, 149 (1998).
[12] W. Zhang *et al.*, Sens. Actuators A, Phys. **102**, 139 (2002).
[13] S. M. Soskin *et al.*, Phys. Rep. **373**, 247 (2003).
[14] A. N. Cleland and M. R. Geller, Phys. Rev. Lett. **93**, 070501 (2004).
[15] B. Yurke *et al.*, Phys. Rev. A **51**, 4211 (1995).
[16] A. H. Nayfeh, *Nonlinear Oscillations* (Wiley, New York, 1979).
[17] M. I. Dykman *et al.*, Phys. Rev. E **49**, 1198 (1994).
[18] G. Gabrielse *et al.*, Phys. Rev. Lett. **54**, 537 (1985).
[19] I. Siddiqi *et al.*, Phys. Rev. Lett. **93**, 207002 (2004).
[20] M. Dykman and M. Krivoglaz, Sov. Phys. JETP **50**, 30 (1979).
[21] A. N. Cleland *et al.*, Appl. Phys. Lett. **79**, 2070 (2001).
[22] K. L. Ekinci *et al.*, Appl. Phys. Lett. **81**, 2253 (2002).
[23] H. A. Kramers, Physica (Utrecht) **7**, 284 (1940).
[24] V. I. Mel'nikov, Phys. Rep. **209**, 1 (1991).
[25] R. L. Kautz, Phys. Lett. A **125**, 315 (1987).
[26] T. A. Fulton and L. N. Dunkleberger, Phys. Rev. B **9**, 4760 (1974).
[27] R. P. Feynman and A. R. Hibbs, *Quantum Mechanics and Path Integrals* (McGraw-Hill, New York, 1965).
[28] W. H. Press, *Numerical Recipes in C* (Cambridge University Press, Cambridge, U.K., 1992).
[29] B. Ilic *et al.*, J. Appl. Phys. **95**, 3694 (2004).